International Journal of Nanoelectronics and Materials
IJNeaM
ISSN 1985-5761 | E-ISSN 2232-1535

Physical Properties of Nanostructured Zinc Sulfide Thin Films Deposited by the PLD Method for Gas Sensing

Suad M. Kadhim[a*], Yasmeen Z. Dawood[b], Esraa K. Hamed[a]

[a] *Laser and Optoelectronics Engineering Department, University of Technology - Iraq*
[b] *Medical physics, collage of science, University of Al-Qadisiyah- Iraq*
**Corresponding author.email: Suad.M.Kadhim@uotechnology.edu.iq*

Received 15 February 2024, Revised 10 March 2024, Accepted 13 March 2024

ABSTRACT

The pulsed laser deposition (PLD) technique created nanostructured semiconducting zinc sulfide (ZnS) thin films onto a quartz substrate. A gas sensing static unit, field emission scanning electron microscopy (FE-SEM), and X-ray diffraction (XRD) were used to analyze the structural, surface morphology, and gas sensing properties of the as-deposited thin films. After the ZnS thin films were formed, they were heated to evaluate the effects of annealing on the characteristics of the ZnS film. XRD analysis reveals that the ZnS thin films exhibit a structure similar to zinc blend cubes, with a preference for the (111) orientation. The X-ray diffraction (XRD) patterns that emerge during annealing show that ZnS thin films become more crystalline. Grain size increases as the annealing temperature rises. Images captured by field emission scanning electron microscopy (FESEM) revealed a grain-like sphere for each of the annealed thin films, confirming the growth of grains. The UV-Vis spectra showed that the ZnS samples' transmittance boosts after annealing because their crystalline quality is improved. The transmittance is measured within the 400−900 nm band, and the optical band gap is direct at 3.72 eV, decreasing to 3.51 eV at 350 °C during annealing. Annealing significantly improves the physical properties of ZnS thin films, according to all presented data. NO_2 and CO_2 gas were used to obtain the I-V values of the samples. The ability of ZnS thin films formed at different annealing temperatures was tested using NO_2 gas. The sensors were fabricated and tested at different operating temperatures and NO_2 gas concentrations of 100, 300, 400, 500, and 700 ppm.

Keywords: *PLD, ZnS, gas sensing, Nanostructure, structure properties, optical properties.*

1. INTRODUCTION

Nanostructured semiconductors have recently gained popularity to enhance the performance of systems such as photocatalysts, photosensors, etc. Zinc sulfide (ZnS) nanostructures have attracted attention for several reasons [1]. Zinc chalcogenide is a type of semiconductor that falls under the IV-VI compound family [2]. At room temperature, this semiconductor material's crystal structure displays a cubic phase (zinc blend); however, at higher temperatures, it transforms into a hexagonal phase (wurtzite) [3]. Zinc Sulfide is considered an n-type semiconductor due to its band-gap value of approximately 3.6 eV. The band gap energy of the cubic phase is 3.68 eV, and that of the wurtzite phase is 3.77 eV, according to the results [4−6]. According to the results of these tests, the band gap of ZnS appears to be reasonably significant. Having qualities that make it highly appealing for use in applications such as light-emitting diodes (LEDs) that emit ultraviolet (UV) light, the comprehensive band-gap material, which is comparable to III-nitrides and their alloys, possesses properties that make it very appealing for use in applications [7], infrared windows (IR) [8], cathodic ray tubes (CRTs) [9], sensors [10 − 12], biological applications [13], and solar cells [14, 15].

It has a refractive index of 2.35, making it a semiconductor [16]. However, zinc sulfide also has a lot of other advantages, such as the fact that it is inexpensive and does not cause any adverse effects. As a result, zinc sulfide (ZnS) can be utilized as the buffer layer in solar cells that are based on copper indium gallium selenide (CIGS) rather than cadmium sulfide (CdS) or cadmium tetrachloride (CdTe) [17]. There are several methods, including thermal evaporation [18], spray pyrolysis [19], molecular beam epitaxy [20], radio frequency reactive sputtering [21], chemical bath deposition [22], photochemical deposition [23], atomic layer deposition [24], and pyrolytic liquid deposition [25 − 27]. PLD might be used for large-scale expansion. The effect of annealing settings on the physical properties of ZnS thin films has aroused significant interest among academics. At a temperature of 400 ℃, the cubic ZnS phase transforms, resulting in the hexagonal ZnS structure, as stated by Ghadri *et al.* [28-30]. For zinc sulfide (ZnS), increasing the annealing temperature from 100 to 500 ℃ increases the crystallite size of the material while simultaneously resulting in a drop in the band gap energy. God, along with other people, made this discovery. They also observed that the annealing procedure enhances zinc sulfide's structural and optical properties (ZnS).

This work aims to analyze the impact of annealing temperature on the structural, morphological, optical, and electrical properties of ZnS thin films, as the conditions under which ZnS films synthesize can affect their characteristics. The reason for this is that the conditions under which ZnS films are synthesized have the potential to affect the properties of the film. Additionally, these membranes can function as sensors for the gases NO_2 and CO_2.

2. EXPERIMENTAL SECTION

The procedure of pulsed laser deposition was utilized to cultivate thin layers of zinc sulfide on a substrate made of quartz; for cleaning the quartz slide with an area of (2 x 2) cm^2 was used and placed in the ultrasonic device was employed for 15 min, where distilled water was first placed, then replaced with ethanol, then distilled water again, and then dried with an air dryer. The target was prepared by compressing high-purity ZnS using a press. The distance between the substrate and the fixed target is 15cm. The operation was conducted in the chamber under 10^{-3} mbar pressure. The Nd-YAG laser was used with some 300 pulses, a wavelength of 532nm, 10Hz, a substrate temperature of 200℃, and an energy pulse of 800 mJ with a focal length of 12cm. During the annealing process, the samples were allowed to cool down before removal. At 350, 450, and 550 ℃, ZnS thin films were annealed in an electric furnace as the final step. The Fizeau optical interference technique was applied to ascertain the thickness of the examined films. This technique was outfitted with a He-Ne laser source and a beam expander. The Equation was utilized to determine the thickness of every film that was produced correctly [31]:

$$t = \frac{\lambda}{2}.\frac{\Delta x}{x} \quad (1)$$

In the given equation [1], the variable (X) represents the width of the fringe, while the variable (ΔX) represents the distance. Research was conducted on ZnS films to investigate their structural, electrical, and optical properties. The nanostructures were obtained by utilizing the quartz substrates; the structural information was obtained by(XRD)using a Rigaku D MAX-2000 powder diffractometer engaging Cu Kα radiation (0.15 = 0.154056 nm) with 2θ in the range (20°−70°). For the purpose of determining the average size of the crystal, Scherer's formula was utilized [3, 16]:

$$G.S = \frac{A\lambda}{\cos\theta\Delta\theta} \quad (2)$$

Where G.S represents the typical size of a crystallite (grain), A constant A is equal to (^1), the wavelength is denoted by λ, Δθ(β) represents the complete width at half maximum of the XRD peaks, and θ represents the Bragg angle during the X-ray diffraction (XRD) analysis. It is also possible to obtain the dislocation density (δ), and the strain (ε) can be estimated by using equations 3 and 4 as well [24]:

$$\delta = \frac{1}{D^2} \quad (3)$$

$$\varepsilon = \frac{\beta\cos\theta}{4} \quad (4)$$

Where D represents the size of the grain, studying the morphology was accomplished with the help of a field emission scanning electron microscope (FE-SEM) manufactured by ZEISS, a German company. This microscope uses a field emission cannon that strictly concentrates high-energy and low-energy electron beams. This results in a significant improvement in both the spatial resolution and the structure's shape.

Equipped with a Cecile CE 7200 Spectrophotometer, ZnS coatings' optical transmission absorption spectra on quartz substrates were measured within the 400–1100 nm range. One may determine the films' absorption coefficient (α) by utilizing the transmission spectrum data, as illustrated in Equation [15, 31].

$$\alpha = \frac{1}{d}\ln\frac{1}{T} \quad (5)$$

Where (T) represents the transmittance and (d) represents the thickness of such film. The following Equation is used to find out the energy gap values of the tin sulfide films [32]:

$$\alpha h\nu = A(h\nu - Eg)^{0.5} \quad (6)$$

Per the Equation (6), where the letter (A) stands for a constant, the letter (α) stands for the absorption coefficient, the letter (υ) stands for the photon frequency, and the letter (h) stands for the constant of Planck.

In order to investigate the sample surface using I-V and gas sensor data, aluminum electrodes were placed in the shape of a comb on the surface of the sampling material. A handmade chamber set on a thermo-controlled hot plate was used to conduct tests on the specifications of NO_2 and CO_2 sensors. All samples are mixed with gas at a concentration of 500 ppm. Then, the best sensitivity of the samples is tested with air at concentrations ranging from 100 ppm to 700 ppm, using controlled flow meters to turn the gas on and off appropriately. By utilizing a computer-connected multi-meter, we could track the change in sample resistance as a function of time in contact with the mixed gas. After measuring the resistance response of each sensor structure, a sensitivity value was calculated using the well-known formula 7 [33]:

$$S = \frac{\Delta R}{R} \quad (7)$$

$$S = \frac{R_{air}}{R_{gas}} \quad (8)$$

3. RESULTS AND DISCUSSION

To understand the impact of the wafer's optical and electrical characteristics, one must measure the thickness of the thin films. As indicated in Table 1, the thickness of the thin films was measured by applying Equation (1) to all samples.

The PLD method involves removing bigger particles from the target surface and depositing them on substrates; the film thickness grows with increasing annealing temperature.

Figure 1 illustrates the X-ray diffraction pattern of ZnS thin film samples grown at three distinct annealing temperatures: 350 ℃, 450 ℃, and 550 ℃. There is a favored orientation in the c (111) diffraction line, which coincides with the intense diffraction peaks displayed by these patterns at around 28.02° . Two miners were observed at (2θ) at 48.1º and 57.5° for all deposition temperatures; they were recognized as c (220) and c (311), respectively, as a result of the predominant plane c (111). As previously stated, XRD confirmed that these crystalline planes correspond to the polycrystalline ZnS phase. One possible explanation for the intense phase signal is the enhancement effect, which occurs when another element's radiation interacts with the specimen's structure to stimulate the analyte element, resulting in secondary radiation [26].

Even though the film thickness that is deposited at 550 ℃ is greter than that which is deposited at 350 ℃ or 450 ℃, the XRD intensity decreases when the temperature is raised to 550 ℃ as a result of the increase in temperature. One can ascertain the average grain size by applying the Scherrer formula, often known as Equation 2. The structural properties of ZnS thin films at various annealing temperatures are listed in Table 1.

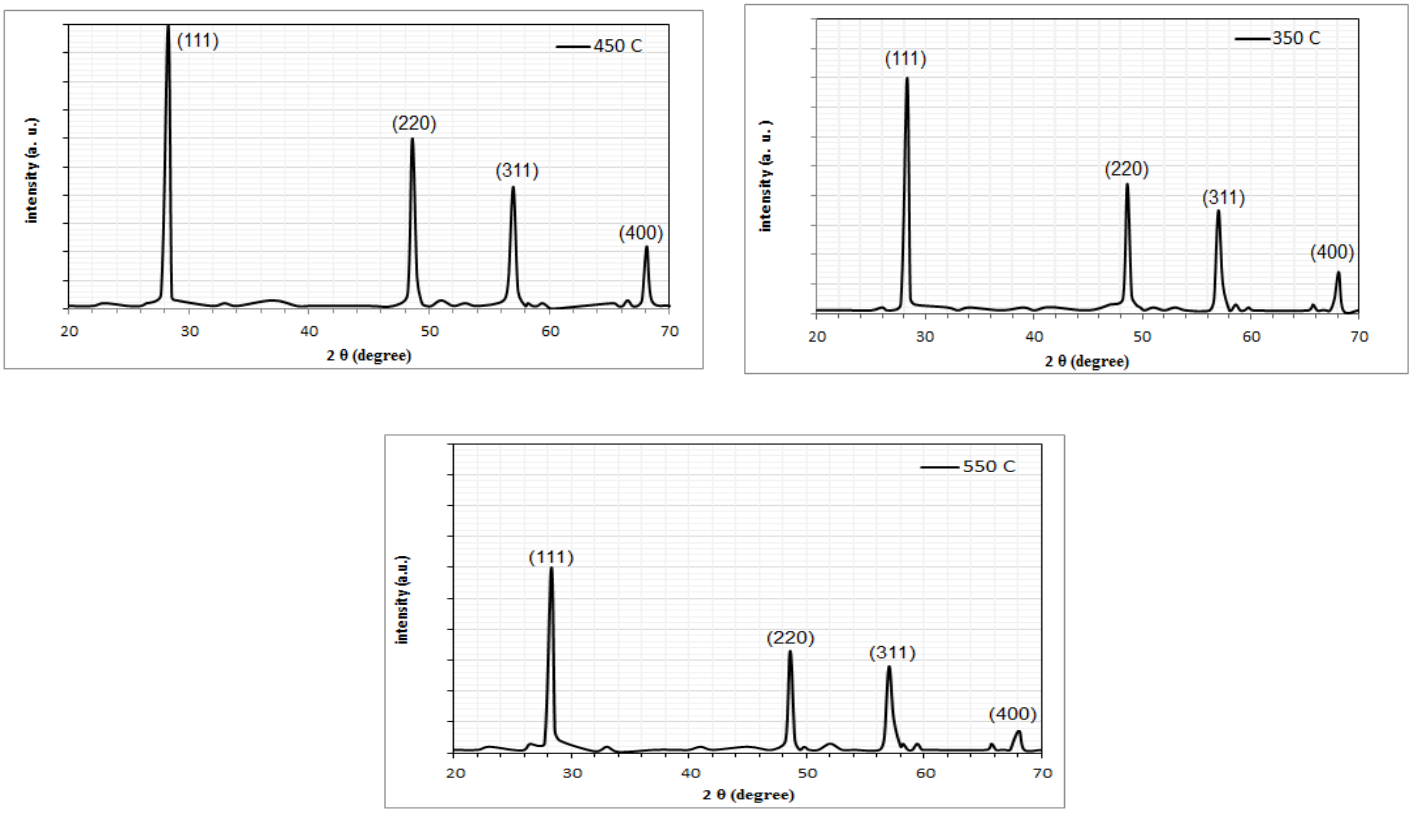

Figure 1 Variations in annealing temperature as seen in the X-ray patterns of ZnS thin films.

Table 1 Properties of the structure and optics of ZnS thin films under varying conditions.

Annealing temp.℃	Thickness (nm)	2 θ (˚)	(hkl) Plane	Eg (eV)	G.S(nm)	δ (× 10^{14}) (lines/m^2)	ε(× 10^{-4})
350	158.43	28.32	111	3.58	37.21	91.74	43.2
450	192.98	28.31	111	3.71	58.85	84.94	41.9
550	220.33	28.35	111	3.50	72.51	76.14	40.2

Figure 2 displays FE-SEM images of ZnS thin films that underwent annealing at 350, 450, and 550 ℃. The fact that almost all of the nanoparticles can be observed on their own or attached to the FE-SEM images proves this is the case.

Images demonstrate that the nanoparticles generate spherical particles at all annealing temperatures. At 350 ℃, the particle distribution generated spherical particles that were uniform and homogeneous. The distribution became less regular at increased annealing temperatures of 450 ℃ and 550 ℃

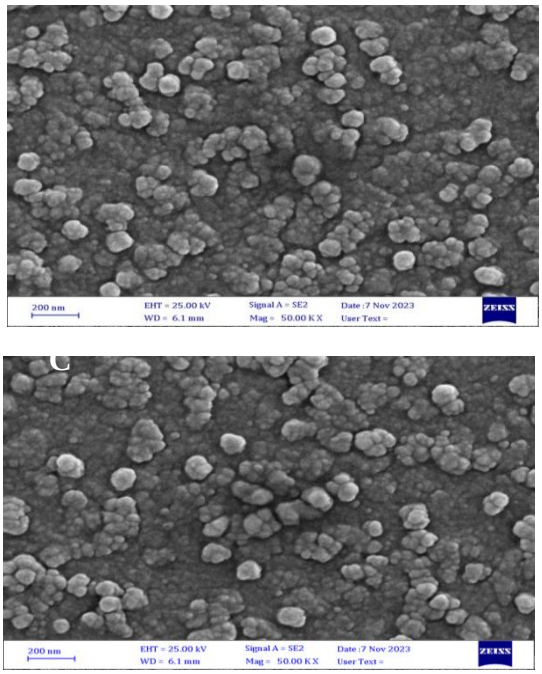

Figure 2 FE-SEM images of ZnS thin films for different annealing temperatures, A) 350℃, B) 450℃, and C) 550℃.

The optical transmittance spectra of ZnS thin films subjected to varying annealing temperatures are shown in Figure 3, with wavelengths ranging from 400 nm to 900 nm. The results demonstrated that, across the board, the transmittance grows as the wavelength increases for all coatings. The transmission of these films is shown to increase dramatically in the range of (510 to 650) nm. Furthermore, all thin films have maximum transmittances ranging from 43.6% to 85.4%, as shown by these graphs. According to the spectra, the transmission increased from a temperature increase from 350 ℃ to 450 ℃. The reason for this is that a larger quantity of light energy is absorbed, which leads to a more significant number of electronic transitions between the valence band and the conduction band on the part of the material [5]. When the annealing temperature approaches 550 ℃, the optical transmittance decreases, and the absorption edge moves to a lower energy area [28]. This is because annealing, which is performed at high temperatures, affects the composition of the film's structure and morphology when it is carried out.

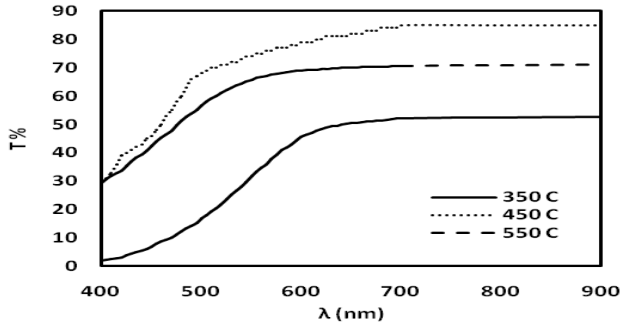

Figure 3 Spectrum of optical transmittance against wavelength for ZnS subjected to varying annealing temperatures.

Because it demonstrates that a film is transparent to radiation with energy below the energy gap (hυ ≤ Eg), the energy gap offers a precise understanding of optical absorption. This is because the energy gap demonstrates that a film absorbs radiation with energy above it (hυ ≥ Eg). To determine the Eg values of the energy gap in the ZnS nanoparticle films, we use Equation (4). For the purpose of estimation, the graph depicting the variables $(\alpha hv)^2$ concerning (hv) can be utilized, as demonstrated in Figure 6. As the annealing temperature increased, the energy band gap readings went from 3.72 to 3.51 eV, indicating a decrease in the energy gap. Overlapping levels are created when the separate levels of unbound atoms widen the energy bands. To understand the impact of the wafer's optical and electrical characteristics, one must measure the thickness of the thin films. As a result, as the temperature of these films rises, their band gaps exhibit many overlapping energy bands. Because overlapping energy bands minimize the energy band gap, band gaps decrease as the annealing temperature gradually increases. Figure 4 provides a visual representation of the influence of annealing conditions on the band gap. The band gap value is determined by extrapolating the straight line that is derived from the plot of $(\alpha hv)^2$ versus photon energy.

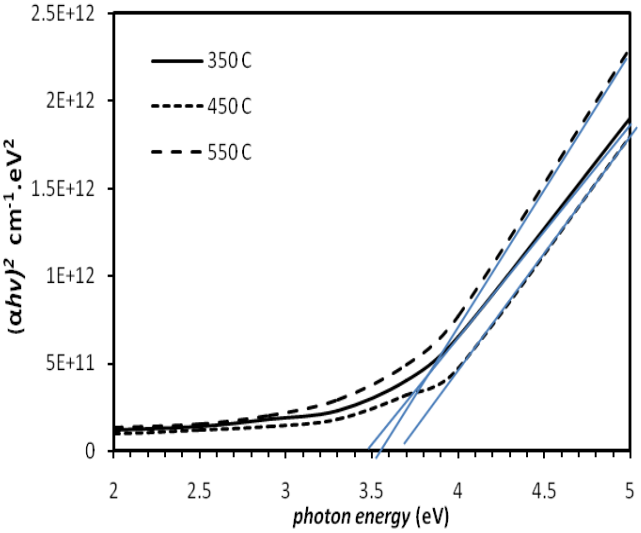

Figure 4 The change in $(\alpha hv)^2$ as a function of photon energy for ZnS thin films subjected to varying annealing temperatures.

3.1. Gas Sensor Measurements

In Figure 5, the voltage and current variations that occurred in the samples are depicted as a function of the presence of air, NO_2, and CO_2 gas. Figure 5 illustrates the relationship between the stacking current and the voltage that is being applied. This article discusses how gas concentration affects the relationship between voltage and current used. While injecting gases, the current levels skyrocketed because oxygen molecules linked themselves to the surface and took electrons from the semiconductor's conduction band [30]. The figure shows that when NO_2 gas entered the samples rather than CO_2 gas and air, the current increased. Again, the relationship was of linear behavior (ohmic relationship).

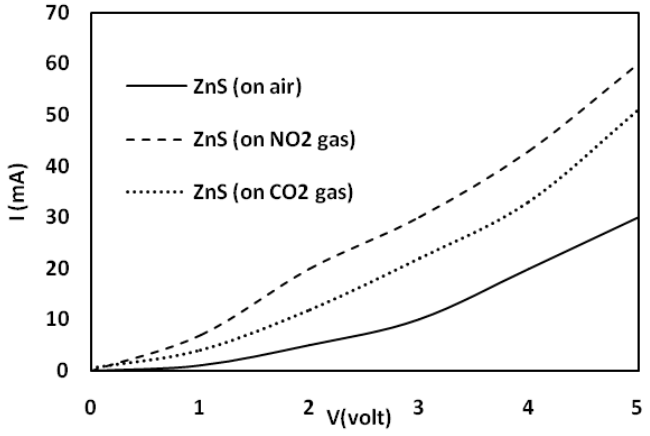

Figure 5 ZnS sensors' current-voltage properties in air, CO_2, and NO_2 gas applications.

Figure 6 illustrates the resistance fluctuation for the ZnS thin films with 500 ppm NO_2 gas. As soon as the gas is introduced, there is a noticeable fall in the electrical resistance, and after some time has passed, there is a noticeable increase in the resistance values. The amount of the usual sensor response to nitrogen dioxide NO_2 changes with the time the sensor is exposed to the gas; it is possible to measure the response of a gas sensor by using Equation (7). The change in conductivity of the sensing materials serves as the foundation for the gas-detecting mechanism that ZnS gas sensors depend upon. The molecules of oxygen are essential to the sensory system's function. As a result of the oxygen molecules attaching themselves to the surface and absorbing electrons from the semiconductor's conduction band, the ZnS material ionizes and takes on the shapes of the molecule oxygen (O_2) and the atom oxygen (O, O_2). When it comes to nitrogen dioxide (NO_2), the mechanism of the ZnS sensor can be explained by the interaction between molecules of nitrogen gas and oxygen species that have been adsorbed (O^-, O_2^-, and O_2) at the top layer of the sensor [11, 33].

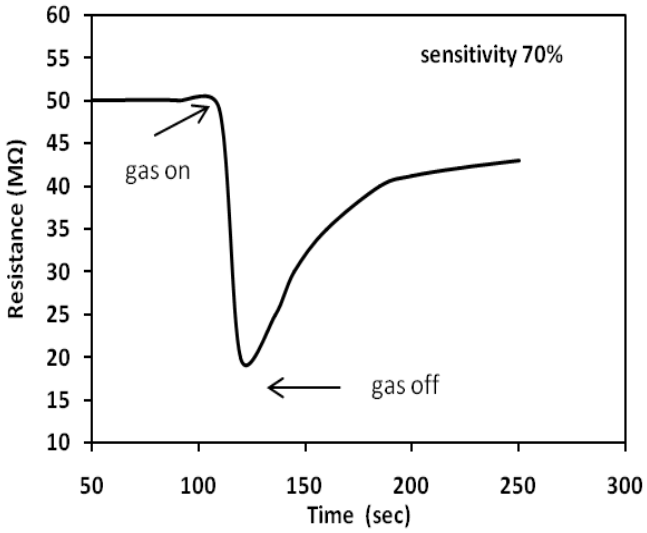

Figure 6 the gaseous sensor ZnS film's resistance to NO_2 at 500 ppm gas amount.

In order to ensure that the sensor is running at the optimal temperature, the effect of the operating temperature was investigated. The sensitivity of the sensor gas was determined by calculating it at a concentration of 500 parts per million (ppm) of both NO_2 and CO_2 gas for a temperature range of (100 − 300) ℃, as depicted in Figure 7. The gas sensitivity rose when the working temperature was raised, hitting a higher value of 72% for NO_2 gas at 250 ℃ and 57% for CO_2 gas at 200 ℃. The working temperature was increased to 300 ℃, which resulted in a diminishment of the sensitivity. At temperatures ranging from 100 to 250 ℃, there is a possibility that an increase in the surface reaction rate contributed to the rise in gas sensitivity. The response might have been reduced if the diffusion depth was low, which occurred when the temperature was raised even higher [32].

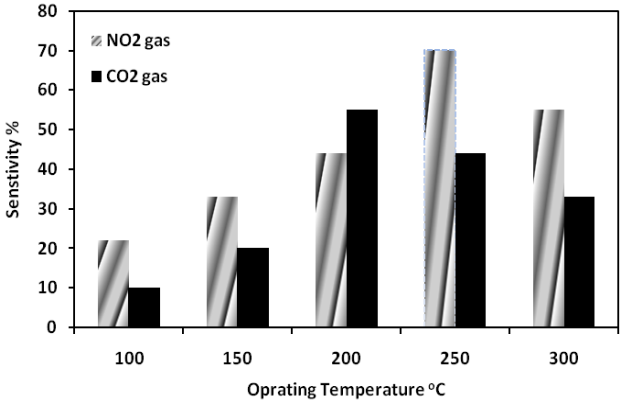

Figure 7 ZnS film sensitivity at variation operating temperature.

Gases of nitrogen dioxide and carbon dioxide were subjected to ZnS thin films produced on zinc sulfur substrates at a range of annealing temperatures to investigate these films' gas-sensing properties. We must know the sensor preparation's specifics to achieve the most significant possible sensitivity values because the created films' sensitivity was evaluated under various preparation requirements. We observed that the maximum value is at a temperature of 550 ℃, which is the optimal temperature of the deposited layer. Figure 8 illustrates the change in sensitivity values caused by the annealing temperature difference. The sensitivity value was significantly higher, given that ZnS films were exposed to NO_2 gas.

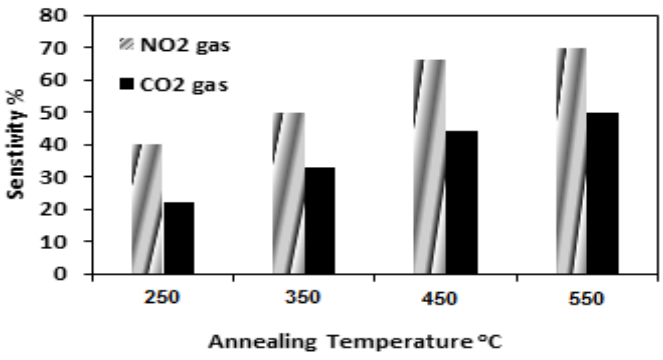

Figure 8 Correlation between annealing temperature and sensitivity changes in ZnS films.

As demonstrated in Figure 9, which reflects a change in sensitivity with increasing concentrations of gas, it is possible to detect that the sensor's sensitivity rose when it was subjected to butane at higher concentration levels. The surface reaction between chemisorbed oxygen and reducing gases is critical to the gas-sensing mechanism's function. Two types of adsorption occur when oxygen is absorbed on the film's surface: physisorption and chemisorption. When the temperature is raised, chemisorption is the predominant process. In order to make the change from physisorption to chemisorption, activation energy is required. This can be achieved by increasing the temperature at which functions are performed.

It has been observed that the amount of oxygen adsorbed on the sensor's surface continues to expand as the temperature rises, reaches its maximum, and then begins to drop as the temperature continues to increase during operation. One can observe the same pattern of behavior in reaction to the gas being examined [32]. The NO_2 gas is detected with an even higher degree of sensitivity by these films.

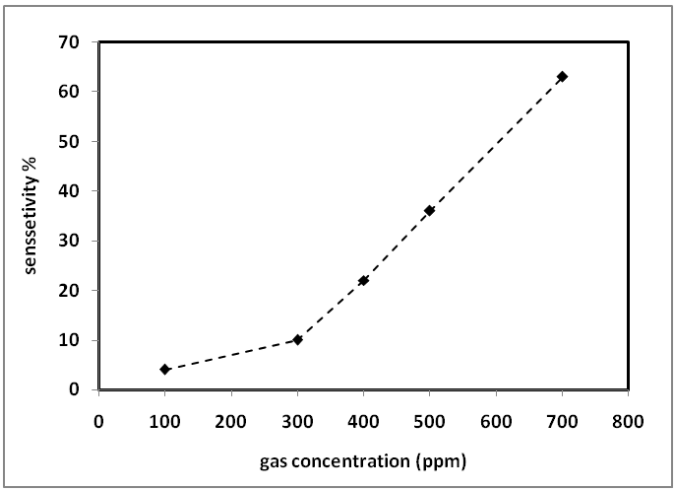

Figure 9. Change of NO_2gas sensitivity with variation in concentration of NO_2 gas.

4. CONCLUSION

ZnS thin film was grown utilizing the PLD method. The structural properties analysis showed that the structures were polycrystalline. With annealing temperatures increasing from 350 ℃ to 550 ℃ respectively, the grain size was increased from 37.21 nm to 72.51 nm, and the FE-SEM images of the prepared ZnS thin films generated spherical particles with a uniform and homogeneous size to look like cauliflower-like morphology. . The synthesized films' XRD styles provide a preferred orientation of the (111) plane. At temperatures of 550 ℃ or higher, under the same conditions as previously, the energy gap steadily narrows, and the energy gap dramatically drops while the particle size grows. As a consequence of the findings, it was proven that nanocrystalline ZnS thin film can be utilized as a novel type of gas-sensing material. At the working temperature, this material is susceptible to NO_2 gas concentrations of 500 ppm. The operational temperature at which the sensor's sensitivity reached its peak value was 250℃. Additionally, the sensitivity of the ZnS sensor will rise as the amount of gas that is introduced increases, up to the point where it reaches its maximum value at 700 parts per million of nitrogen dioxide.

REFERENCES

[1] A. B. Alwany, G. M. Youssef, O. M. Samir, M. A. Algradee, N. A. A. Yahya, M. A. Swillam, S. Humaidi, and R. Abd-Shukor, "Annealing temperature effects on the size and band gap of ZnS quantum dots fabricated by co-precipitation technique without capping agent," *Scientific Reports*, vol. 13, no. 10314, 2023. doi: 10.1038/s41598-023-37563-6.

[2] A. U. R. Khan, M. Ramzan, M. F. Iqbal, M. Hafeez, M. M. Fadhali, H. H. Somaily, M. J. Muhammad, W. Mukhtar, and M. F. Saleem, "Effect of the Source-to-Substrate Distance on Structural, Optoelectronic, and Thermoelectric Properties of Zinc Sulfide Thin Films," *Materials*, vol. 15, no. 22, p. 8047, 2022. doi: 10.3390/ma15228047.

[3] Y. Z. Dawood, "Influence of Ar gas on optical and morphology properties of films (CdS) prepared by pulse laser deposition (PLD) technique," *Int. J. Nanoelectron. Mater.*, vol. 15, no. 1, pp. 9–16, 2022.

[4] M. Y. Nadeem and W. Ahmed, "Optical Properties of ZnS Thin Films," *Turk J Phys*, vol. 24, pp. 651-659, 2000.

[5] M. A. Fakhri, Y. Al-Douri, U. Hashim, and E. T. Salim, "Optical investigations of photonics lithium niobate," *Sol. Eng.*, vol. 120, p. 381, 2015.

[6] S. Al-Jawad, M. M. R. Imran, and N. J. Imran, "Effect of electrolyte solution on structural and optical properties of TiO2 grown by iodization technique for photoelectrocatalytic application," *Surf. Rev. Lett.*, vol. 25, no. 7, p. 1850078, 2018.

[7] J. Ke, S. Chen, L. Song, P. Zhang, X. Cao, B. Wang, and R. Zhang, "Effect of film thickness on structural and optical properties of ZnS:Cu films prepared by vulcanization," *Superlattices and Microstructures*, vol. 146, p. 106671, Oct. 2020. doi: 10.1016/j.spmi.2020.106671.

[8] A. D. F. Ali, A. A. Ali, and W. K. K. Wafaa, "Photodetector fabrication based on heterojunction of CuO/SnO2/Si nanostructures," *Bull. Mater. Sci.*, vol. 45, no. 84, 2022. doi: 10.1007/s12034-022-02672-x.

[9] S. M. H. Al-Jawad, S. H. Sabeeh, A. A. Taha, and H. A. Jassim, "Effect of electrolyte solution on structural and optical properties of TiO2 grown by iodization technique for photoelectrocatalytic application," *J. Sol-Gel Sci. Techn.*, vol. 87, no. 3, p. 362, 2018. doi: 10.1007/s10971-018-4724-9.

[10] H. A. Badran, R. K. F. Alfahed, A. T. Y. Abbas, and A. L. Mghames, "Gas-sensing performance enhancement in ZnS/polymer films by homogenous morphology surface," *J. Phys.: Conf. Ser.*, vol. 1999, p. 012066, 2021. doi: 10.1088/1742-6596/1999/1/012066.

[11] E. T. Salim, R. A. Ismail, M. A. Fakhri, B. G. Rasheed, and Z. T. Salim, "Synthesis of cadmium oxide/Si heterostructure for two-band sensor application," *Iran. J. Sci. and Tech., Transactions A: Science*, vol. 43, no. 3, p. 1337, 2019.

[12] F. A. Mahmoud and G. Kiriakidis, "Nanocrystalline ZnO thin film for gas sensor application," *Journal of Ovonic Research*, vol. 5, no. 1, pp. 15-20, Feb. 2009.

[13] R. C. Ramola, S. Negi, M. Rawat, R. C. Singh, and F. Singh, "Annealing Effects on Gas Sensing Response of Ga-Doped ZnO Thin Films," *ACS Omega*, vol. 6, pp. 11660-11668, 2021. doi: 10.1021/acsomega.1c00984.

[14] R. A. Ismail, N. Hasan, and S. S. Shaker, "Preparation of Bi2Sr2CaCu2Ox thin film by pulsed laser deposition for optoelectronic devices application," *Silicon*, vol. 14, no. 6, pp. 2625-2633, 2022.

[15] Z. Ahmed, T. Rahman, K. M. A. Hussain, M. T. Khatun, M. S. S. Chowdhury, T. Faruqe, F. T. Z. Toma, Y. Ahmed, M. N. I. Khan, and M. M. Alam, "Characterization and optimization of ZnS thin film properties synthesis via chemical bath deposition method for solar cell buffer layer," *Main Group Chemistry*, vol. 22, no. 1, pp. 79-91, 2023. doi: 10.3233/MGC-210127.

[16] R. A. Ismail, N. F. Habubi, and A. N. Abd, "Morphological, Structural and Chemical Properties of p-type Porous Silicon Produced by Electrochemical Etching," *Int. J. Thin Film Sci. Tec*, vol. 3, no. 3, pp. 121-128, 2014.

[17] Y. Z. Dawood, "The Influence of substrate temperature on CdS thin films properties prepared by pulse laser deposition on glass substrates," *Energy Procedia*, vol. 119, pp. 536-544, 2017. doi: 10.1016/j.egypro.07.073.

[18] H. Ghasemi, M. H. Mozaffari, and R. Moradian, "Effects of deposition time on structural and optical properties of ZnS and ZnS/Au thin films grown by thermal evaporation," *Physica B: Condensed Matter*, vol. 627, p. 413616, Feb. 2022. doi: 10.1016/j.physb.2021.413616.

[19] Z. A. Muhammad, A. T. Hassan, and Y. Z. Dawood, "Studying the optical properties of CdO and CdO: Bi thin films," *Baghdad Sci. J.*, vol. 13, no. 3, pp. 395-398, 2016. doi: 10.21123/bsj.13.3.0593.

[20] B. Abdallah, K. Alnama, and F. Nasrallah, "Deposition of ZnS thin films by electron beam evaporation technique, effect of thickness on the crystallographic and optical properties," *Modern Physics Letters B*, vol. 33, no. 4, p. 1950034, 2019. doi: 10.1142/S0217984919500349.

[21] S. F. Hassan, O. A. Chichan, Z. S. A. Mosa, S. S. Chiad, and N. F. Habubi, "Structural and Optical Characterization of Nanostructured Zinc sulfide Thin Films deposited by CBD," *International Journal of Mechanical Engineering*, vol. 7, no. 1, Jan. 2022.

[22] M. Gunasekaran, R. Gopalakrishnan, and P. Ramasamy, "Deposition of ZnS thin films by photochemical deposition technique," *Materials Letters*, vol. 58, no. 1-2, pp. 67-70, Jan. 2004.

[23] J. Koaib, N. Bouguila, H. Abassi, N. Moutia, M. Kraini, A. Timoumi, C. Vázquez-Vázquez, K. Khirouni, and S. Alaya, "Dielectric and electrical properties of annealed ZnS thin films. The appearance of the OLPT conduction mechanism in chalcogenides," *RSC Adv.*, vol. 10, pp. 9549-9562, 2020. doi: 10.1039/c9ra10284a.

[24] R. A. Ismail, A. M. Mousa, K. S. Khashan, M. H. Mohsin, and M. K. Hamid, "Synthesis of PbI nanoparticles by laser ablation in methanol," *Journal of Materials Science: Materials in Electronics*, vol. 27, pp. 10696-10700, 2016.

[25] S. M. Kadhim, "Effect of deposition parameters on kinematics growth and optical properties of Fe2O3 nano films deposited by PLD," *J. Made. Alel. Coll.*, vol. 11, no. 1, 2019.

[26] Y. Z. Dawood, S. M. Kadhim, and A. Z. Mohammed, "Structure and optical properties of nano PbS thin film deposited by pulse laser deposition," *Eng. Tech. J.*, vol. 32, no. 9, pp. 1723-1730, 2015.

[27] M. M. Ali, "Effect of annealing temperature on the structural and optical properties of ZnS thin films deposited by CBD," *Basrah Journal of Science (A)*, vol. 33, no. 1, pp. 156-181, 2015.

[28] M. Asghar, K. Mahmood, S. B. M. Samaa, S. Rabia, and M. Y. Shahid, "Effect of annealing temperature on the structural and optical properties of ZnS thin films," *Materials Today: Proceedings*, vol. 2, pp. 5430-5435, 2015.

[29] B. A. Khanegahi and H. Sedghi, "Effect of Annealing Temperature on Optical Properties of ZnS Thin Films Studied by Spectroscopic Ellipsometry Analysis Method," *International Journal of Nano Research*, vol. 1, no. 2, 2018.

[30] Y. Z. Dawood, "Study the effect of laser energy change on optical and properties of Fe2O3 thin films deposited by PLD technique," *ARPN J. Eng. Appl. Sci.*, vol. 16, no. 12, pp. 1218-1224, 2021.

[31] A. A. Najim, H. H. Darwoysh, Y. Z. Dawood, S. Q. Hazaa, and A. T. Salih, "Structural, topography, and optical properties of Ba-doped MN3O4 thin films for ammonia gas sensing application," *Phys. Stat. Solidi A*, 2018. doi: 10.1002/pssa.201800379.

[32] M. S. Shinde, S. S. Samanta, M. S. Sonawane, P. B. Ahirrao, and R. S. Patil, "Gas Sensing Properties of Nanostructured ZnS Thin Films," *J. Nano. Adv. Mat.*, vol. 3, no. 2, pp. 99-106, 2015. doi: 10.12785/jnam/030203.

[33] Y. Z. Dawood, "A study of the optical and structural properties of the PbS films that affect the sensitivity of the NO2 gas sensor," *J. Opt.*, 25 July 2023. doi: 10.1007/s12596-023-01312-9.